Physics of organic ferroelectric field-effect transistors

Brondijk, Jakob J.; Asadi, Kamal; Blom, Paul W. M.; de Leeuw, Dago M.

Published in:
Journal of Polymer Science. Part B: Polymer Physics

DOI:
10.1002/polb.22363

Publication date:
2012

Physics of Organic Ferroelectric Field-Effect Transistors

Jakob J. Brondijk,[1] Kamal Asadi,[1,2] Paul W. M. Blom,[1,3] Dago M. de Leeuw[1,2]

[1]Molecular Electronics, Zernike Institute for Advanced Materials, University of Groningen, Nijenborgh 4, 9747 AG, Groningen, The Netherlands

[2]Philips Research Laboratories, High Tech Campus 4, 5656 AE Eindhoven, The Netherlands

[3]TNO Holst Centre, P.O. BOX 8550, 5605 KN Eindhoven, The Netherlands

Correspondence to: J. J. Brondijk (E-mail: j.j.brondijk@rug.nl)

Received 1 September 2011; accepted 2 September 2011; published online 20 September 2011
DOI: 10.1002/polb.22363

ABSTRACT: Most of the envisaged applications of organic electronics require a nonvolatile memory that can be programmed, erased, and read electrically. Ferroelectric field-effect transistors (FeFET) are especially suitable due to the nondestructive read-out and low power consumption. Here, an analytical model is presented that describes the charge transport in organic FeFETs. The model combines an empirical expression for the ferroelectric polarization with a density dependent hopping charge transport in organic semiconductors. Transfer curves can be calculated with parameters that are directly linked to the physical properties of both the comprising ferroelectric and semiconductor materials. A unipolar FeFET switches between a polarized and depolarized state, and an ambipolar FeFET switches between two stable polarized states. A good agreement between experimental and calculated current is obtained. The method is generic; any other analytical model for the polarization and charge transport can be easily implemented and can be used to identify the origin of the different transconductances reported in the literature. © 2011 Wiley Periodicals, Inc. J Polym Sci Part B: Polym Phys 50: 47–54, 2012

KEYWORDS: charge transport; conjugated polymers; ferroelectricity; ferroelectrics; field-effect transistors; fluoropolymers; modeling; nonvolatile memory; organic electronics; thin films

INTRODUCTION Organic electronics has emerged as a promising technology for large-area microelectronic applications such as rollable displays and contactless identification transponders or smart labels.[1] Most of these applications require memory functions, preferable a nonvolatile memory that retains its data when the power is turned off, and that furthermore can be programmed, erased and read-out electrically. Ferroelectric field-effect transistors (FeFETs) are attractive for this purpose due to fast nondestructive data read-out and low power consumption.[2,3] A ferroelectric material exhibits a bistable, remnant polarization that can be switched by electric fields exceeding the coercive field. The layout of a FeFET comprises a metal-ferroelectric-semiconductor layer stack [Fig. 1(b)], in which the ferroelectric layer serves as the gate dielectric. The ferroelectric layer, because of its remnant polarization, can adopt either of two stable polarization states, which persist when no biases are applied. Switching from one polarization state to the other can occur by applying a gate bias exceeding the coercive field. Depending on the orientation of the polarization, positive or negative charges are induced in the semiconductor at the semiconductor/ferroelectric interface, that is, in the semiconductor channel. The induced surface charge density shifts the onset of channel accumulation toward either more negative or positive gate bias. Hence, a gate bias window, defined by the shifted onset voltages, exists wherein the drain current may have either of two levels depending on the actual polarization state of the ferroelectric gate dielectric. The corresponding drain current levels can be used to define Boolean "0" and "1" states of a nonvolatile memory with nondestructive read-out.[3] The most commonly used organic ferroelectric material in FeFETs is the random copolymer poly(vinylidenefluoride-*co*-trifluorethylene) (P(VDF-TrFE)), as illustrated in Figure 1(c). The coercive field is about 60 MV/m and the remnant polarization about 60 mC/m^2.[4,5]

The first functional organic FeFET was demonstrated in 2005.[6] Since then many FeFETs using different organic and metal oxide semiconductors have been reported.[7–13] A typical transfer curve of a unipolar *p*-type FeFET is presented in Figure 1(d). Qualitatively the current voltage dependence can be understood as follows. At the beginning of the sweep, the ferroelectric is unpolarized. Current starts to flow at the switch-on voltage, here at around a gate bias of 0 V. Upon increasing negative gate bias the ferroelectric polarizes. The drain current gradually increases as a result of both the linear and the ferroelectric polarization. At ~ -20 V the coercive field is reached, and the ferroelectric is fully polarized. The

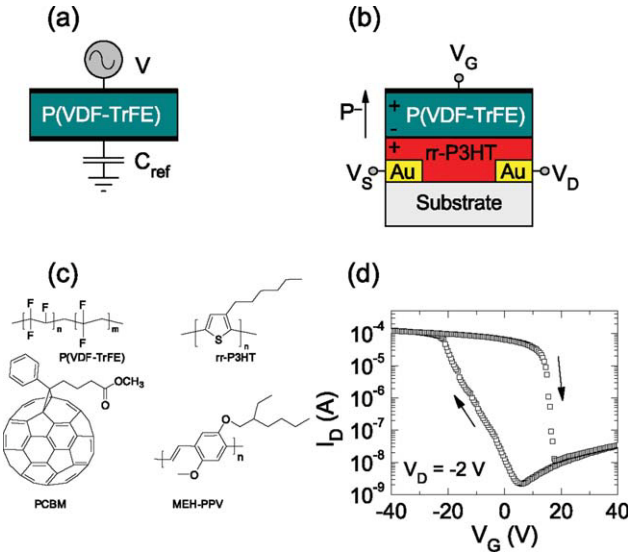

FIGURE 1 Schematic device layout for: (a) A ferroelectric capacitor using P(VDF-TrFE) in a Sawyer-Tower circuit where a reference capacitor C_{ref} in series is used to measure the displacement charge. (b) A ferroelectric field-effect transistor (FeFET) with rr-P3HT as semiconductor and Au source-drain electrodes. The polarization direction resulting in the high conductance state is indicated as *P*. (c) Chemical structure of the used organic materials. (d) Experimental transfer curve of a *p*-type FeFET where the arrows indicate the scan direction.

ferroelectric polarization is saturated and does not change anymore. A further increase of the gate bias only leads to an increase of the accumulated charge carrier density by the linear polarization. Hence, the current hardly increases. Upon scanning back the ferroelectric remains polarized and the current remains high. At a gate bias around +20 V, the coercive field is reached and the ferroelectric polarization changes sign. Because of the contacts electrons cannot be injected in the *p*-type semiconductor. The current in the off-state is low. The transistor behaves as a bi-stable memory; at 0 V gate bias the current in the on-state and the off-state differ by more than 4 decades. Details of the device physics however remain elusive. For instance, what is the contribution of the linear and the ferroelectric polarization to the drain current, and is the polarization stable in the off-state. To answer these questions, a quantitative analysis is needed, which until now has not been reported for organic FeFETs.

The charge transport in inorganic field-effect transistors has been quantitatively been described. The ferroelectric polarization was taken into account by an empirical description. Conventional charge transport theory was applied for the inorganic semiconductor. The operation of the FeFET was modeled numerically; a good agreement was obtained.[14,15]

Translating the methodology to organic FeFETs is not straightforward. Contrary to inorganic semiconductors, the charge carrier mobility in organic semiconductors depends on carrier density. A full description of both polarization of the organic ferroelectric and charge transport of the organic semiconductor is required. Here, we adopt an empirical polarization description that has been successfully used to describe inorganic ferroelectrics. We apply the method to the organic ferroelectric capacitor. With three parameters, we can describe the polarization of the capacitor as a function of bias and history.

To describe the charge transport of an organic FeFET, an analytical description of the charge transport in the organic semiconductor is needed. Here we use a standard model for charge transport based on variable range hopping of charge carriers in an exponential density of localized states.[16] The transport is determined separately in nonferroelectric, conventional field-effect transistors as a function of applied bias and temperature. The transport is quantitatively described with parameters that are directly linked to the physical properties of the semiconductor such as the width of the density of states. We combine the polarization and charge transport descriptions into an analytical, physically-based, direct current (DC) model for organic FeFETs. A good agreement between experimental and calculated transfer curves is obtained. The differences are discussed. We note that the method is generic, any other analytical model for the polarization and charge transport can be implemented.

CHARGE TRANSPORT IN FeFETs

Ferroelectric Polarization section presents the first ingredient to model the charge transport in organic FeFETs, *viz.* the description of the polarization behavior in discrete capacitors as a function of applied field and history. With four parameters, we can fully describe the electrical displacement. Subsequently, the charge transport in the bare semiconductor is investigated in conventional field-effect transistors as a function of applied bias and temperature. The transport is quantitatively described by a standard hopping model, with parameters that are directly linked to the physical properties of the semiconductor such as the width of the density of states. We combine the two descriptions into a unified analytical model for organic FeFETs. The charge transport in both unipolar and ambipolar FeFETs is calculated and compared with the experimental data.

Ferroelectric Polarization

The input for modeling the charge transport in an organic FeFET is an electrical description for the polarization of the ferroelectric gate dielectric. Therefore, we fabricated capacitors of P(VDF-TrFE) and measured the electric displacement as a function of electric field. The displacement *D* is the sum of the linear dielectric polarization and the ferroelectric polarization and is given by:

$$D = \varepsilon_0 \varepsilon_F E + P(E) \tag{1}$$

where ε_0 is the vacuum permittivity, ε_F the relative permittivity, *E* the electric field over the ferroelectric and *P* the ferroelectric polarization. Figure 2 shows the displacement for increasing values of the maximum applied electric field. We

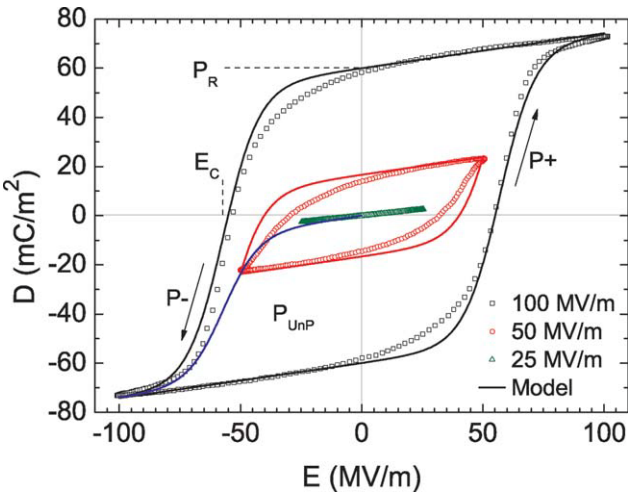

FIGURE 2 Displacement versus applied electric field for a ferroelectric P(VDF-TrFE) capacitor. The scan direction is indicated by the arrows. The displacement was subsequently measured up to 25, 50, and 100 MV/m and presented as the green, red, and black dots, respectively. The solid lines are fits to the experimental data.

start from an unpolarized ferroelectric. When the applied field remains much lower than the coercive field only the linear dielectric polarization contributes (green triangles). The displacement is symmetric and the lack of hysteresis indicates that there is no ferroelectric polarization. The relative permittivity, ε_F, was determined as 16 in good agreement with literature values.[17] Upon increasing the maximum applied electric field up to the coercive field, E_C, the inner displacement loops shows hysteresis (red circles). The ferroelectric polarization increases with maximum electric field, until the polarization and the hysteresis loop saturate (blue line). The maximum amount of polarization within the ferroelectric, P_S, has been reached (black squares). At zero applied field a remnant polarization P_R remains, which is constant in time as long as depolarization can be disregarded.

We use a reported empirical, analytical description for the saturated and unsaturated polarization as a function of electric field.[14,15] We start with an unpolarized ferroelectric. The polarization in the first initial measurement is then given by:

$$P(E) = \frac{P_S}{2}\left(\tanh\left(\frac{E+E_C}{\delta}\right) + \tanh\left(\frac{E-E_C}{\delta}\right)\right) \quad (2)$$

with

$$\delta \equiv 2E_C\left(\ln\left(\frac{1+\frac{P_R}{P_S}}{1-\frac{P_R}{P_S}}\right)\right)^{-1} \quad (3)$$

After the first measurement, the ferroelectric is partly polarized. The polarization depends on the maximum applied electric field, E_{max}. Subsequent measurements at lower fields do not change the polarization state of the ferroelectric. These measurements then yield the inner displacement loops. The polarization as a function of field, below the previously applied maximum field is given by:

$$P^+(E,E_{max}) = P_S\tanh\left(\frac{E-E_C}{\delta}\right) + \frac{P_S}{2}\left(\tanh\left(\frac{E_{max}+E_C}{\delta}\right) - \tanh\left(\frac{E_{max}-E_C}{\delta}\right)\right) \quad (4)$$

$$P^-(E,E_{max}) = P_S\tanh\left(\frac{E+E_C}{\delta}\right) - \frac{P_S}{2}\left(\tanh\left(\frac{E_{max}+E_C}{\delta}\right) - \tanh\left(\frac{E_{max}-E_C}{\delta}\right)\right) \quad (5)$$

where P^- (P^+) denotes polarization towards negative (positive) polarization, as specified in Figure 1(b). When the maximum field gets much larger than the coercive field the ferroelectric polarization saturates. The saturated polarization follows from eqs 4 and 5 for $E_{max} >> E_C$ and is given as a function of applied electric field, E, as:

$$P^+(E) = P_S\left(\frac{E-E_C}{\delta}\right) \quad (6)$$

$$P^-(E) = -P^+(-E) \quad (7)$$

The displacement loops can be fitted by adding the linear dielectric displacement to the appropriate ferroelectric polarization. The black curve in Figure 2 is the saturated displacement fitted to the experimental data measured at a maximum electric field of 100 MV/m. A good agreement is obtained using parameter values $P_R = 59.95$ mC/m^2, $P_S = 60$ mC/m^2, $E_C = 57$ MV/m. The values correspond to typical values found for P(VDF-TrFE) capacitors.[4,5,18,19] A measured value of $\varepsilon_F = 16$ was assumed to be frequency and electric field independent. By keeping the four polarization parameters fixed, both the inner loops for the partially polarized ferroelectric and the first initial scan for the unpolarized ferroelectric can be calculated. The blue and red lines are calculated and both show a good description of the experimental data. The differences especially below E_C are due to the simple empirical model used. To derive an improved description is beyond the scope of this work. We note however, that any other analytical formula that yields a better fit can easily be implemented in the charge transport model of the FeFET.

Charge Transport in Organic Transistors

Charge transport in organic semiconductors is governed by thermally activated hopping of charge carriers between localized sites at the Fermi level. The density of the localized states (DOS) can be approximated by a Gaussian or an exponential energy distribution. The Fermi level determines the local occupation of the DOS, that is, the charge carrier density. With increasing carrier density, hopping becomes more favorable and the mobility increases. To determine the charge transport properties as a function of carrier density, we fabricated separately conventional field-effect transistors of a typical organic semiconductor, regio-regular poly-3-

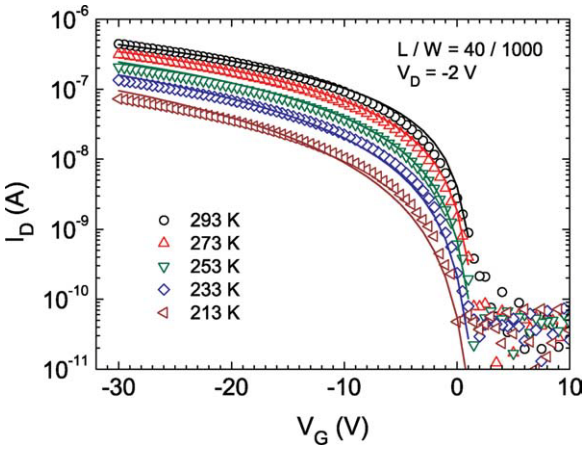

FIGURE 3 Linear transfer curves of an organic field-effect transistor using rr-P3HT as semiconductor, measured as a function of temperature. The symbols represent the experimental data. The solid lines are fits to the data.

hexylthiophene (rr-P3HT), as illustrated in Figure 1(c). SiO_2 was used an inert, nonferroelectric gate dielectric. The linear transfer curves as a function of temperature are presented in Figure 3. The hysteresis is negligible. The Au source and drain electrodes on rr-P3HT form an Ohmic contact for holes resulting in a unipolar *p*-type transistor. At negative gate, bias holes are accumulated and the current is enhanced. At positive gate bias the semiconductor is depleted from charge carriers, electrons cannot be injected, and the current is negligible.

There are various models for the charge transport. Here we use a standard charge transport model based on variable range hopping in an exponential density of localized states.[16] Contact resistances and charge trapping are disregarded. Using the gradual channel approximation, an expression for the drain current in a unipolar transistor is then given by:[20]

$$I_D = \frac{W}{qL}\sigma_0 f C^{2T_{rel}-1}\frac{1}{2T_{rel}-1}\frac{1}{2T_{rel}}\left(\frac{1}{2k_B T_0 \varepsilon_{sc}\varepsilon_0}\right)^{T_{rel}-1} \times\left(\|V_{eff}\|^{2T_{rel}}-\|V_{eff}+V_D\|^{2T_{rel}}\right) \quad (8)$$

with the prefactor f defined as:

$$f\left(\frac{T_{rel}^4 \sin\left(\frac{\pi}{T_{rel}}\right)}{(2\alpha)^3 B_C}\right)^{T_{rel}} \quad (9)$$

where σ_0 is a conductivity prefactor, α^{-1} is an effective overlap parameter, B_C is related to the onset of percolation and given by 2.8 for three-dimensional systems and $T_{rel} = T_0/T$, where T_0 is a characteristic temperature describing the width of the density of states. C is the gate capacitance per unit area and ε_{sc} is the dielectric constant of the semiconductor. The elementary charge is denoted by q and the vacuum permittivity by ε_0. Holes are accumulated at negative gate bias, beyond the switch-on voltage (V_{SO}) where V_{SO} is the gate bias at flat band.[21] The effective gate bias is then $V_{eff} = -V_G + V_{SO}$. The notation $\|u\| \equiv \frac{1}{2}(|u|+u)$ is included in eq 8 to ensure that the calculated current in depletion is zero.

The solid lines in Figure 3 represent a fit to the transfer curves. For all temperatures, a good agreement is obtained. The capacitance of the SiO_2 gate dielectric was 17 nF cm^{-2} and ε_{sc} was taken as 3. The fit parameters were determined as $\sigma_0 = 2.86 \times 10^6$ S/m, $T_0 = 350$ K, $\alpha^{-1} = 2.6$ Å, and $V_{SO} = 2$ V. The room temperature mobility determined at a gate bias of -30 V was 0.03 cm^2/Vs, which is a typical value for rr-P3HT.[22,23]

The transport parameters are later determined in actual FeFETs as well. The possible differences then might be related to changes in physical properties of the semiconductor such as in the density of states or in the mobility prefactor due to dipolar disorder. We note that we use a standard hopping model. Details such as the influence of deep trap states are not included. However, any other analytical equation that yields an improved description of the charge transport can easily be implemented.

Combined Description of a FeFET

Here we combine the description for the ferroelectric polarization with that of the charge transport in organic semiconductors. The polarization of the ferroelectric film in a FeFET depends on the electric field over the ferroelectric, induced by the gate bias. We focus on the linear operating regime of the transistor, that is, $|V_G| >> |V_D|$. We use the gradual channel approximation; the electric field in the direction perpendicular to the channel is much larger than the source-drain field. Hence, the electric field is taken to be independent on the position in the channel. We approximate the field by $E = \frac{V_G - V_{SO}}{d_F}$ where d_F is the thickness of the ferroelectric. The polarization is calculated from the electric field. Depending on the history and scan direction, the applicable description of the ferroelectric polarization, $P(V_G)$ is chosen from eqs 2, 4–7. The polarization corresponds to a surface charge density. As a consequence of Gauss's law, an interface charge at the dielectric-semiconductor interface leads to a shift of the switch-on voltage.[24] Here, we include the ferroelectric polarization as a gate dependent shift of the switch-on voltage. The effective gate bias V_{eff} used in eq 8 is therefore replaced by:

$$V_{eff}^* = -V_G + V_{SO} - \frac{P(V_G)}{C} \quad (10)$$

Introduction of the expression for the effective gate bias combines the descriptions of ferroelectric polarization with the charge transport.

Charge Transport in a Unipolar FeFET

Unipolar FeFETs were fabricated using rr-P3HT as a *p*-type semiconductor and P(VDF-TrFE) as a ferroelectric gate insulator. The linear transfer curve is presented in the bottom panel of Figure 4. The gate bias was swept from +35 to −35 V and back. The ferroelectric layer thickness was

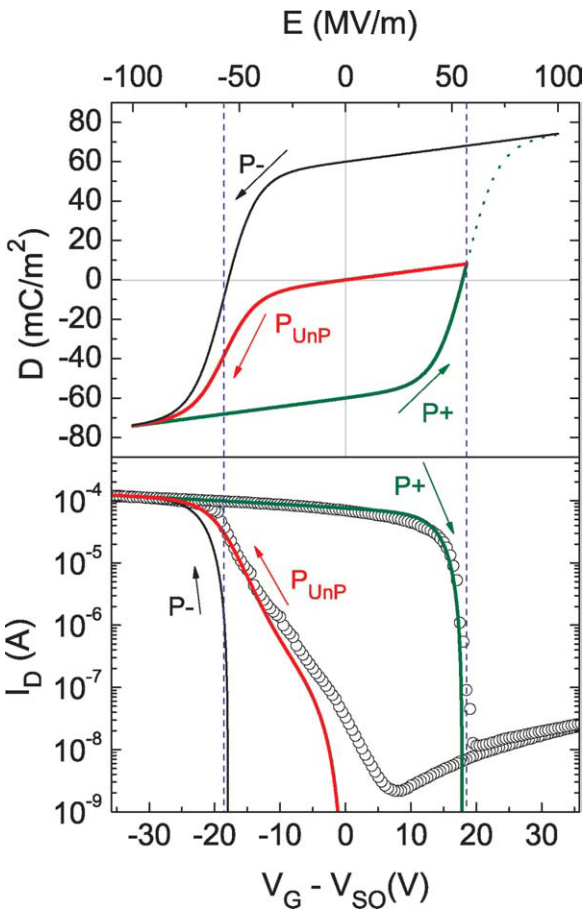

FIGURE 4 (top) Calculated displacement charge of a ferroelectric capacitor as a function of the applied electric field. (bottom) Linear transfer curve of a rr-P3HT FeFET. The drain bias was −2 V. The channel length and width were 20 and 10000 μm. The ferroelectric layer thickness was 325 nm. Symbols represent experimental data and the lines are model predictions.

325 nm. Hence, the maximum gate field exceeds the coercive field. At the beginning of the sweep, the ferroelectric is unpolarized. Upon increasing negative gate bias beyond ~−20 V, the ferroelectric gets fully polarized. A high hole density is induced at the semiconductor-ferroelectric interface and a high current is measured. Upon scanning back, the ferroelectric remains polarized. The current remains high, the FeFET is in the on-state. At a gate bias around +20 V, the coercive field is reached and the ferroelectric polarization changes sign. Electron injection into the *p*-type semiconductor is severely hampered due to the use of Au source and drain contacts. The current in the off-state is low.

The question is if the ferroelectric in the off-state is polarized or depolarized. To stabilize the polarization at positive gate, bias electrons are required. The electron current is negligible. Hence, the ferroelectric polarization cannot be compensated, and the ferroelectric depolarizes to the pristine state. The measurement therefore is reproducible; the same source-drain current loop is measured in a subsequent sweep.

For completeness and to verify the presented methodology, the transfer curves were measured while increasing the maximum negative gate bias from −15 V in steps of 5 to −50 V. The corresponding linear transfer curves are presented in Figure 5. The hysteresis in the drain current increases with maximum applied gate bias until the saturated ferroelectric polarization has been reached.

Modeling the Charge Transport in a Unipolar FeFET

By connecting the effective gate bias with the ferroelectric polarization, we can calculate the linear transfer curves. Because the polarization depends on the history of applied biases and the applied gate bias, the applicable description of the ferroelectric polarization has to be taken. The parameters describing the polarization, viz. the remnant polarization, saturated polarization, coercive field and relative permittivity, were taken from the fit of the displacement versus field of the P(VDF-TrFE) capacitor as described above (Fig. 2): $P_R = 59.95$ mC/m^2, $P_S = 60$mC/m^2, $E_C = 57$MV/m and $\varepsilon_F = 16$. The calculated expected displacement is presented in the upper part of Figure 4. The pristine ferroelectric is unpolarized. Upon increasing negative bias, the ferroelectric gets polarized (P_{UnP}), and the polarization saturates beyond the coercive field, at a gate bias of about −20 V. On scanning back, the ferroelectric remains polarized (P^+) up to a gate bias of +20 V, corresponding to the coercive field, where it switches back to the unpolarized, pristine state.

We assume that the remnant polarization (P_R) and the coercive field (E_C) are the same for the ferroelectric in a capacitor and in a transistor. Hence, the values determined from the capacitor measurements were used to model the

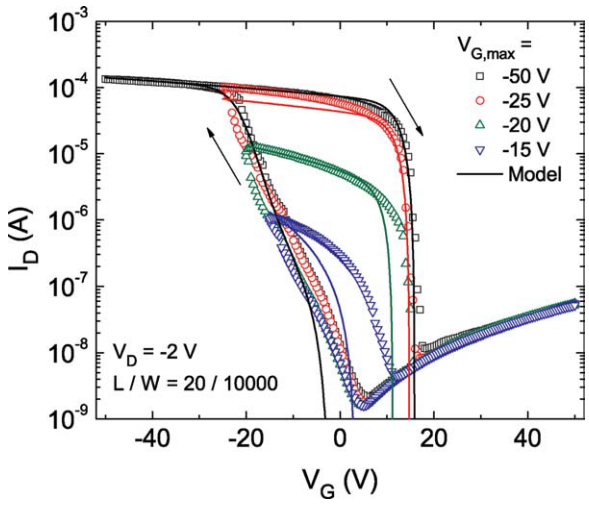

FIGURE 5 Linear transfer curves of a rr-P3HT FeFET. The sweep direction is indicated by the arrows. The ferroelectric layer thickness was 325 nm. The gate bias was swept to a maximum negative gate bias from −15 V in steps of 5 to −50 V, and back to + 30 V. The symbols represent the experimental currents. The solid lines are model predictions.

polarization in the FeFET. By including the charge-transport parameters determined from the unipolar rr-P3HT transistor of Figure 2, the transfer curve of the FeFET in Figure 4 can be predicted. However, when using the same values the current in the FeFET is overestimated. To achieve a close fit to the measured FeFET current, an effective mobility of about a factor of 3 lower had to be used. For the optimal fit of Figure 4, we used $\sigma_0 = 6 \times 10^5$ S/m, $T_0 = 450$ K, $\alpha^{-1} = 2.6$ Å, and $V_{SO} = -2$ V. The solid red line holds for the unpolarized ferroelectric (P_{UnP}) and the solid green line for the saturated polarization (P^+). A good agreement is obtained. The inner current loops of Figure 5 can be calculated as well. Because the applied maximum bias is below the coercive field, the ferroelectric is only partially polarized. Hence, for the back scan, eq 4 has to be used. The solid lines in Figure 5 are calculated. A reasonable agreement is obtained. The deviations are mainly due to inaccuracies in the simple empirical description of the ferroelectric polarization, especially below the coercive field E_C. To derive an improved description of the inner loop polarization is beyond the scope of this work. We note however, that any other analytical equation that yields a better fit can easily be implemented in the expression for the effective gate bias. Second, we assume a uniform polarization along the channel. The calculation of the current therefore is only strictly valid for the linear operating regime. Hence, deviations in the saturated and subthreshold regimes can be expected.

We note that the ferroelectric switches between a polarized on-state and a depolarized off-state. As an illustration, we calculated the current assuming that the off-state is also fully polarized (P^-). The black line in Figure 4 shows indeed a striking disagreement with the experimentally measured current.

The effective mobility in the FeFET is a factor of 3 lower than that in the corresponding conventional transistor. The differences are due to a decreased prefactor and an increased width of the density of states. The increased width of the DOS might indicate dipolar disorder in the FeFET. The decreased prefactor might be due to a field-effect mobility that decreases with increasing dielectric constant.[25,26]

The present description of a FeFET might be used to explain issues reported in literature. In the first FeFETs, it was argued that the ferroelectric polarization in a FeFET is about a factor 3 lower than in ferroelectric capacitor.[6] However, using the presented model we show that the reduced current in these early FeFETs could be equally due to a lower effective mobility. A definite answer can be given from the analysis of the full temperature dependence. The same holds for reported FeFETs that show large differences in transconductance. For instance, the mobility of pentacene[9] and of triisopropyl-silylethynyl pentacene (TIPS-PEN) in FeFETs is reported to be different from that in state-of-the-art regular field-effect transistors.[11,27,28] The present analytical description might be used to analyze where the differences are coming from.

Modeling the Charge Transport in an Ambipolar FeFET

The first ambipolar ferroelectric transistor was reported in 2005.[29] P(VDF-TrFE) was used as a ferroelectric and a mixture of poly(2-methoxy-5-(2′-ethylhexyloxy)-*p*-phenylene vinylene) (MEH-PPV) and [6,6]-phenyl-C_{61}-butyric acid methyl ester (PCBM) as the semiconductor. Both materials are illustrated in Figure 1(c). Au was used as source and drain contact. Because Au can inject holes in MEH-PPV and electrons in PCBM, ambipolar charge transport was observed. The experimental linear transfer curves are reproduced in Figure 6. The arrows indicate the scan direction. The transfer curve of the ambipolar FeFET shown in Figure 6 exhibits a characteristic "butterfly" shape: starting in the *p*-channel mode the application of a positive gate voltage leads to a decrease of the channel (hole) current. When the gate field approaches the coercive field of the ferroelectric, the transistor switches from the *p*-mode into the *n*-mode, leading to a sharp increase in the current. A negative gate bias suppresses the electron current until the hole current switches on. The transistor operates as in a *p*-type or *n*-type mode depending on the bias history and has therefore a programmable polarity.

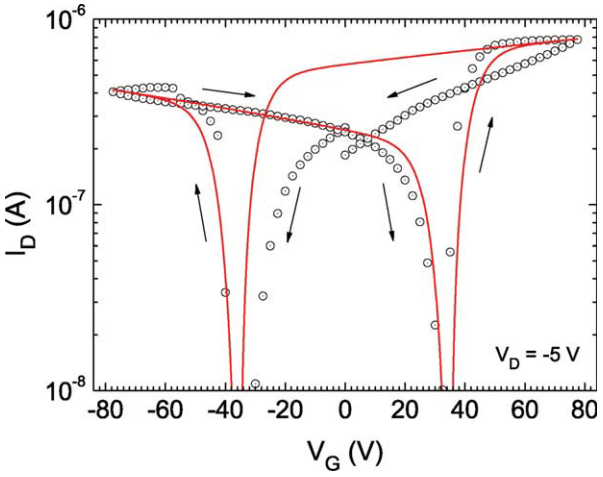

FIGURE 6 Linear transfer curve of an ambipolar FeFET reproduced from Ref. [29] (symbols). A layer of P(VDF-TrFE) with a thickness of 900 nm was used as a ferroelectric gate dielectric. A mixture of MEH-PPV and PCBM was used as the semiconductor. The arrows indicate the scan direction. The solid lines are fits to the experimental data. The transport parameters for the hole transport were: $\sigma_{0,p} = 1 \times 10^5$ S/m, $T_{0,p} = 540$ K, and $\alpha_p^{-1} = 1.4$ Å. For the electron transport $\sigma_{0,n} = 4 \times 10^5$ S/m, $T_{0,n} = 400$ K, and $\alpha_n^{-1} = 1.05$ Å were used. The switch-on voltage was fixed at 0 V.

Because both holes and electrons can be accumulated in the channel both polarization states of the ferroelectric can be compensated. Both polarization states are stable, depolarization can be disregarded. Upon applying gate biases exceeding the coercive field, the ferroelectric switches between the two fully polarized states. For modeling the ferroelectric polarization, we used expressions for the fully saturated polarizations. We assumed that the remnant and saturated polarization of the ferroelectric are the same as measured in a capacitor. A lower value for the coercive field of $E_C = 40$ MV/m was used. The electron current can be described

similar as the hole current (eq 8) by substituting opposite bias polarities:

$$I_{D,n} = \frac{W}{qL}\sigma_{0,n} f_n C^{2T_{rel,n}-1} \frac{1}{2T_{rel,n}-1}\frac{1}{2T_{rel,n}}\left(\frac{1}{2k_B T_{0,n}\varepsilon_{sc}\varepsilon_0}\right)^{T_{rel,n}-1} \times \left(\left\|-V^*_{eff}\right\|^{2T_{rel,n}} - \left\|-V^*_{eff} - V_D\right\|^{2T_{rel,n}}\right) \quad (11)$$

where the subscript *n* indicates the electron transport parameters: $T_{0,n}$, $\sigma_{0,n}$, and α_n^{-1}. To calculate the current we used reported transport parameters for MEH-PPV and PCBM.[30,31] We only adapted the prefactor for the mobility, σ_0. The calculated current is presented by the solid red curve in Figure 6. A good agreement is obtained. However, the used prefactor is two orders of magnitude lower than the reported prefactor. This means that the charge transport in the reported ambipolar FeFET is hampered by the unoptimized device processing. P(VDF-TrFE) is a semi-crystalline polymer, hence unoptimized processing yields rough films. The roughness of the ferroelectric gate is directly related to a lower field-effect mobility, as reported in literature.[32] We note that due to the high relative permittivity of P(VDF-TrFE) the DOS of the semiconductor can be locally broadened.[25] The value of T_0 is related to the DOS. A much closer fit to the data can indeed be achieved by using a higher value for $T_{0,n}$ (not shown). Irrespective of the discrepancies, the analysis clearly shows that the ferroelectric in an ambipolar transistor switches between two stable polarized states.

CONCLUSIONS

We have presented an analytical model to describe the charge transport in organic FeFETs. Key elements are an empirical reported method to describe the polarization in ferroelectric capacitors and a separate description of the charge transport in organic semiconductors. Upon connecting the effective gate bias with the ferroelectric polarization, the transfer curves in an organic FeFET could analytically be calculated. For both unipolar and ambipolar FeFETs, a good agreement has been obtained with parameters that are directly linked to the physical properties of both the comprising ferroelectric and semiconductor materials. Differences are mainly due to the simple empirical model for the polarization. However, any other analytical model for the polarization and for the charge transport can easily be implemented. A unipolar FeFET switches between a polarized and a depolarized state, and an ambipolar FeFET switches between two stable polarized states. The model can be used to identify the origin of the different transconductances reported in the literature. The present model calculates the direct current for a discrete FeFET. It can be directly extended to an AC model that can be implemented in standard circuit simulators to design ferroelectric memory arrays.

EXPERIMENTAL

The ferroelectric random copolymer poly(vinylidenefluoride-co-trifluoroethylene) (65–35%) (P(VDF-TrFE)) was purchased from Solvay, Belgium and was used as received. Regio-regular poly(3-hexyl thiophene) (rr-P3HT) was purchased from Rieke Metals. Rr-P3HT was purified before use, by dissolving in distilled toluene, dedoped with hydrazine and precipitating in methanol. The fraction collected was Soxhlet extracted with methanol, n-hexane, and dichloromethane until the extraction solvent was colorless. The dichloromethane fraction was precipitated in methanol, collected, dissolved in chloroform and precipitated again in methanol. The collected fraction was dried under vacuum and stored under a N_2 atmosphere.

Ferroelectric capacitors were fabricated on glass substrates with Ag bottom electrodes. A layer of P(VDF-TrFE) was spin coated onto the substrates from a methylethylketon (MEK) solution (30–50 mg/mL). Before spin coating the solution was filtered using a 1-μm PTFE filter. The film thickness was 300–400 nm as measured with a Dektak profilometer. The films were subsequently annealed at 140 °C in a vacuum oven (10^{-1} mbar) to enhance the crystallinity of P(VDF-TrFE). A top contact of Ag was evaporated through a shadow mask to finish the capacitors. The device area was 1 × 1 mm^2. The ferroelectric capacitors were characterized using a home-built Sawyer-Tower circuit, as shown in Figure 1(a), at a frequency of 100 Hz.

Unipolar, nonferroelectric transistors were fabricated on a heavily doped silicon monitor wafer acting as a common gate electrode. Thermally grown SiO_2 passivated with hexamethyldisilazane was used as gate dielectric. The SiO_2 thickness was 200 nm. Source and drain electrodes of Au (100 nm) were defined using conventional photolithography, with Ti (10 nm) as an adhesion layer. The channel width was 1000 μm. To minimize the influence of short-channel effects and contact resistance, channel lengths larger than 10 μm were used. A film of rr-P3HT was spin coated from a chloroform solution (5–10 mg/mL), after the solution was filtered with a 0.2-μm PTFE filter. The semiconductor thickness was 80 nm and the film was annealed in a vacuum oven at 140 °C.

Unipolar ferroelectric transistors were fabricated on thermally oxidized Si monitor wafers using a bottom contact top gate structure. Source and drain electrodes of Au were defined as described above. The channel length varied from 5 to 40 μm, whereas the channel width was kept constant at 10000 μm. A film of rr-P3HT was spin coated from chloroform and subsequently a P(VDF-TrFE) layer was spin coated from MEK. We note that MEK is an orthogonal solvent for rr-P3HT. The film thicknesses were 30 nm for rr-P3HT and 300–400 nm for P(VDF-TrFE). The stack was annealed in a vacuum oven at 140 °C. To form the staggered top gate of the FeFETs, a 70-nm Ag layer was evaporated through a shadow mask. Electrical characterization of the transistors was performed in vacuum (10^{-5} mbar) using a Keithley 4200 semiconductor characterization system.

ACKNOWLEDGMENT

We gratefully acknowledge J. Harkema and F. van der Horst for technical support. We thank R. C. G. Naber for making

experimental data available. We acknowledge financial support from the Zernike Institute for Advanced Materials and by the EC under FP7 contract no. 212311, ONE-P.

REFERENCES AND NOTES

1 Cantatore, E.; Geuns, T. C. T.; Gelinck, G. H.; van Veenendaal, E.; Gruijthuijsen, A. F. A.; Schrijnemakers, L.; Drews, S.; de Leeuw, D. M. *IEEE J Solid-State Circuits* **2007,** *42*, 84–92.

2 Setter, N.; Damjanovic, D.; Eng, L.; Fox, G.; Gevorgian, S.; Hong, S.; Kingon, A.; Kohlstedt, H.; Park, N. Y.; Stephenson, G. B.; Stolitchnov, I.; Taganstev, A. K.; Taylor, D. V.; Yamada, T.; Streiffer, S. *J. Appl. Phys.* **2006,** *100*, 051606-1–051606-46.

3 Naber, R. C. G.; Asadi, K.; Blom, P. W. M.; de Leeuw, D. M.; de Boer, B. *Adv. Mater.* **2010,** *22*, 933–945.

4 Lovinger, A. J. *Science* **1983,** *220*, 1115–1121.

5 Takahashi, T.; Date, M.; Fukada, E. *Appl. Phys. Lett.* **1980,** *37*, 791–793.

6 Naber, R. C. G.; Tanase, C.; Blom, P. W. M.; Gelinck, G. H.; Marsman, A. W.; Touwslager, F. J.; Setayesh, S.; de Leeuw, D. M. *Nat. Mater.* **2005,** *4*, 243–248.

7 Naber, R. C. G.; de Boer, B.; Blom, P. W. M.; de Leeuw, D. M. *Appl. Phys. Lett.* **2005,** *87*, 203509-1–203509-3.

8 Gelinck, G. H.; Marsman, A. W.; Touwslager, F. J.; Setayesh, S.; de Leeuw, D. M.; Naber, R. C. G.; Blom, P. W. M. *Appl. Phys. Lett.* **2005,** *87*, 092903-1–092903-3.

9 Lee, K. H.; Lee, G.; Lee, K.; Oh, M. S.; Im, S.; Yoon, S.-M. *Adv. Mater.* **2009,** *21*, 4287–4291.

10 Kang, S. J.; Bae, I.; Shin, Y. J.; Park, Y. J.; Huh, J.; Park, S. -M.; Kim, H. -C.; Park, C. *Nano Lett.* **2011,** *11*, 138–144.

11 Kang, S. J.; Bae, I.; Park, Y. J.; Park, T. H.; Sung, J.; Yoon, S. C.; Kim, K. H.; Choi, D. H.; Park, C. *Adv. Funct. Mater.* **2009,** *19*, 1609–1616.

12 Park, C. H.; Lee, K. H.; Lee, B. H.; Sung, M. M.; Im, S. *J. Mater. Chem.* **2010,** *20*, 2638–2643.

13 Zheng, Y.; Ni, G.-X.; Toh, C.-T.; Zeng, M.-G.; Chen, S.-T.; Yao, K.; Özyilmaz, B. *Appl. Phys. Lett.* **2009,** *94*, 163505-1–163505-3.

14 Miller, S. L.; McWhorter, P. J. *J. Appl. Phys.* **1992,** *72*, 5999–6010.

15 Lue, H.-T.; Wu, C.-J.; Tseng, T.-Y. *IEEE Trans. Electron Devices* **2002,** *49*, 1790–1798.

16 Vissenberg, M. C. J. M.; Matters, M. *Phys. Rev. B* **1998,** *57*, 12964–12967.

17 Park, Y.; Bae, I.-S.; Kang, S.; Chang, J.; Park, C. *IEEE Trans. Dielectr. Electr. Insul.* **2010,** *17*, 1135–1163.

18 Yamada, T. *J. Appl. Phys.* **1981,** *52*, 6859–6863.

19 Shrestha, B.; Pieper, R.; Wondmagegn, W.; Satyala, N. Proceedings of IEEE Southeastcon 2011, Nashville, TN, **2011,** 224–227.

20 Smits, E. C. P.; Anthopoulos, T. D.; Setayesh, S.; van Veenendaal, E.; Coehoorn, R.; Blom, P. W. M.; de Boer, B.; de Leeuw, D. M. *Phys. Rev. B* **2006,** *73*, 205316-1–205316-9.

21 Meijer, E. J.; Tanase, C.; Blom, P. W. M.; van Veenendaal, E.; Huisman, B.-H.; de Leeuw, D. M.; Klapwijk, T. M. *Appl. Phys. Lett.* **2002,** *80*, 3838–3840.

22 Chang, J.-F.; Clark, J.; Zhao, N.; Sirringhaus, H.; Breiby, D.; Andreasen, J.; Nielsen, M.; Giles, M.; Heeney, M.; McCulloch, I. *Phys. Rev. B* **2006,** *74*, 115318-1–115318-12.

23 Bao, Z.; Dodabalapur, A.; Lovinger, A. J. *Appl. Phys. Lett.* **1996,** *69*, 4108–4110.

24 Possanner, S. K.; Zojer, K.; Pacher, P.; Zojer, E.; Schürrer, F. *Adv. Funct. Mater.* **2009,** *19*, 958–967.

25 Veres, J.; Ogier, S. D.; Leeming, S. W.; Cupertino, D. C.; Mohialdin Khaffaf, S. *Adv. Funct. Mater.* **2003,** *13*, 199–204.

26 Richards, T.; Bird, M.; Sirringhaus, H. *J. Chem. Phys.* **2008,** *128*, 234905-1–234905-5.

27 Kim, D. H.; Lee, D. Y.; Lee, H. S.; Lee, W. H.; Kim, Y. H.; Han, J. I.; Cho, K. *Adv. Mater.* **2007,** *19*, 678–682.

28 Park, S. K.; Jackson, T. N.; Anthony, J. E.; Mourey, D. A. *Appl. Phys. Lett.* **2007,** *91*, 063514-1–063514-3.

29 Naber, R. C. G.; Blom, P. W. M.; Gelinck, G. H.; Marsman, A. W.; de Leeuw, D. M. *Adv. Mater.* **2005,** *17*, 2692–2695.

30 Tanase, C.; Meijer, E. J.; Blom, P. W. M.; de Leeuw, D. M. *Phys. Rev. Lett.* **2003,** *91*, 216601-1–216601-4.

31 Anthopoulos, T. D.; Tanase, C.; Setayesh, S.; Meijer, E. J.; Hummelen, J. C.; Blom, P. W. M.; de Leeuw, D. M. *Adv. Mater.* **2004,** *16*, 2174–2179.

32 Steudel, S.; De Vusser, S.; de Jonge, S.; Janssen, D.; Verlaak, S.; Genoe, J.; Heremans, P. *Appl. Phys. Lett.* **2004,** *85*, 4400–4402.